Supplementary Information

Reticular synthesis of two anionic Zn(II)-MOFs for organic dyes adsorption/separation and lanthanide ions sensitization

Hao Zhang, Wu-Yue Geng, Yu-Hui Luo,* Zi-Jun Ding, Zhi-Xuan Wang, A-Di Xie, Dong-En Zhang*

School of Environmental and Chemical Engineering, Jiangsu Ocean University, Lianyungang 222000, P. R. China.

* Corresponding authors. E-mail: luoyh@jou.edu.cn (Yu-Hui Luo),
2007000040@jou.edu.cn (Dong-En Zhang)

Materials and Measurements

All reagents and solvents were purchased from commercial sources and used without purification. H_4TCPB and H_3BPTC were prepared according to the literature.[1, 2] Powder X-ray diffraction (PXRD) patterns were collected on a PANalytical X'Pert Powder X-ray diffractometer with graphite monochromatized Cu *Kα* radiation (λ = 0.15418 nm), 2θ ranging from 3 to 50 º with an increment of 0.02 º, and a scanning rate of 10 º/min. The FT-IR spectra were measured by using KBr pellets in the range 4000 - 400 cm^{-1} on a Thermo Scientific spectrometer. The UV-vis absorption was measured with a PERSEE UV-vis-NIR spectrophotometer. The fluorescent spectroscopy was measured on a FL-7000 HITACHI luminescence spectrometer at room temperature with a light source of Xenon lamp.

X-ray crystallography

Crystallographic diffraction data for **JOU-44** and **JOU-45** were recorded on a Bruker Apex CCD diffractometer with graphite monochromatized Mo-*Kα* radiation (λ = 0.71073 Å) at room temperature. Both structures were solved by Direct Method of

SHELXS-2018 and refined by full-matrix least-squares techniques by using the SHELXL-2018 program.[3] All nonhydrogen atoms were refined with anisotropic temperature parameters. All hydrogen atoms were placed in geometrically idealized position as a riding mode. The solvent molecules and $[Me_2NH_2]^+$ cations in the crystal are highly disordered and are removed by using the SQUEEZE routine of PLATON.[4] For **JOU-44**, ISOR command was used to restrict some of the atoms. For **JOU-45**, SADI, DFIX, SIMU and ISOR commands were used to restrict some of the atoms and bond length, whereas AFIX 66 was used to restrict the geometry of benzene ring of the ligand. For both **JOU-44** and **JOU-45**, weak diffraction intensities at high angel result in the Alert A THETM01 and PLAT029. The crystallographic data for **JOU-44** and **JOU-45** were summarized in Table S1, and the selected bond lengths and angles are listed in Table S2 and S3.

Table S1. Crystallographic data and structure refinements of **JOU-44** and **JOU-45**.

Compounds	**JOU-44**	**JOU-45**
Formula	$C_{16.25}H_{15.75}N_{1.25}O_6Zn$	$C_{26}H_{36}N_{3.5}O_{9.5}Zn$
Formula weight	389.92	614.95
Crystal system	Orthorhombic	Orthorhombic
Space group	*Pbam*	*Pbam*
a (Å)	25.411(12)	17.693
b (Å)	16.573(8)	33.688
c (Å)	16.573	16.248
α (°)	90	90
β (°)	90	90
γ (°)	90	90
V (Å^3)	6980(5)	9684(3)
Z	8	8
Density (g cm^{-3})	0.742	0.844
F(000)	1600	2580
Crystal Size (mm)	0.35*0.31*0.12	0.33 * 0.31 * 0.12
2θ (°)	2.458 - 41.382	2.418 - 36.858
Reflections	18506	24442
Data/restraints/parameters	3275 / 30 / 200	3714 / 556 / 278
GOF on F^2	1.035	1.018
R_1, wR_2 [I > 2σ (I)]	0.0727, 0.1934	0.1094, 0.2837
R_1, wR_2 (all data)	0.1067, 0.2033	0.1534, 0.3234

[a] $R_1 = \sum||F_0| - |Fc||/\sum|F_0|$; $wR_2 = \sum[w(F_0^2 - Fc^2)^2]/\sum[w(F_0^2)^2]^{1/2}$.

Table S2. Selected bond lengths (Å) and angels (°) for **JOU-44.**

Zn_1-$O_3{}^1$	1.921(7)	Zn_2-$O_6{}^3$	1.887(7)
Zn_1-$O_8{}^2$	1.930(6)	Zn_2-$O_7{}^2$	1.887(7)
Zn_1-O_8	1.930(6)	Zn_2-O_7	1.903(8)
Zn_1-$O_5{}^3$	1.991(7)	Zn_2-O_1	1.930(9)
$O_3{}^1$-Zn_1-$O_8{}^2$	110.6(2)	O_7-Zn_2-$O_7{}^2$	110.4(5)

O_3^1-Zn_1-O_8	110.6(2)	O_7-Zn_2-O_1	113.7(2)
O_8^2-Zn_1-O_8	115.7(4)	O_7^2-Zn_2-O_1	113.7(2)
O_3^1-Zn_1-O_5^3	98.4(3)	O_7-Zn_2-O_6^3	109.8(3)
O_8^2-Zn_1-O_5^3	110.1(2)	O_7^2-Zn_2-O_6^3	109.8(3)
O_8-Zn_1-$O5^3$	110.1(2)	O_1-Zn_2-O_6^3	98.6(4)

Symmetry transformations: [1] 1/2 + x, 1/2 - y, 2 - z; [2] +x, +y, 2 - z; [3] 1 - x, -y, 2 - z.

Table S3. Selected bond lengths (Å) and angels (°) for **JOU-45.**

Zn_1-O_7^1	1.825(14)	Zn_2-O_2^2	1.882(12)
Zn_1-O_1^2	1.914(11)	Zn_2-O_2	1.882(12)
Zn_1-O_1	1.914(11)	Zn_2-O_5^3	1.892(11)
Zn_1-O_3	1.940(13)	Zn_2-O_4	1.905(14)
O_7^1-Zn_1-O_1^2	113.7(4)	O_2-Zn_2-O_2^2	112.2(7)
O_7^1-Zn_1-O_1	113.7(4)	O_2^2-Zn_2-O_5^3	114.6(4)
O_1^2-Zn_1-O_1	109.5(7)	O_2-Zn_2-O_5^3	114.6(4)
O_7^1-Zn_1-O_1^3	97.2(7)	O_2^2-Zn_2-O_4	108.9(4)
O_1^2-Zn_1-O_3	111.1(4)	O_2-Zn_2-O_4	108.9(4)
O_1-Zn_1-O_3	111.1(4)	O_5^3-Zn_2-O_4	96.0(5)

Symmetry transformations: [1] -1/2 + x, 1/2 - y, 1 - z; [2] +x, +y, 1 - z; [3] 2 - x, 1 - y, 1 - z.

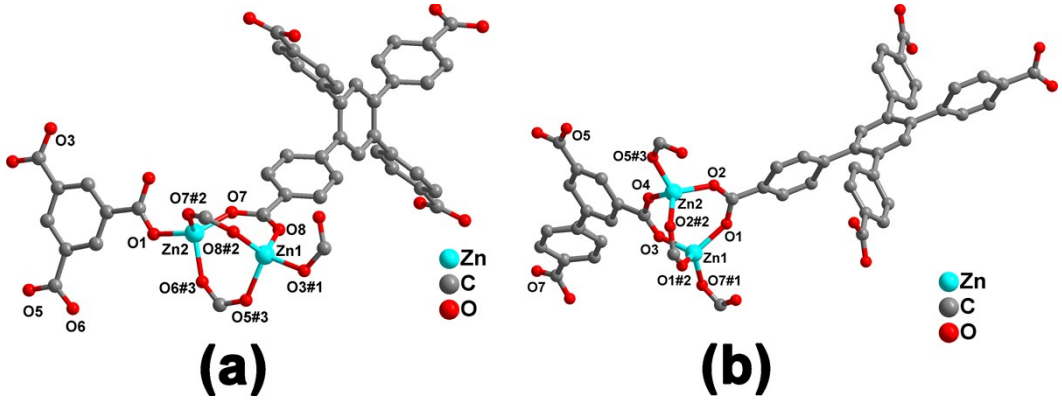

Fig. S1. (a) Coordination environment of Zn ions in **JOU-44**. Symmetry code: [#1] 1/2 + x, 1/2 - y, 2 - z; [#2] +x, +y, 2 - z; [#3] 1 - x, -y, 2 - z. (b) Coordination environment of Zn ions in **JOU-45**. Symmetry code: [#1] -1/2 + x, 1/2 - y, 1 - z; [#2] +x, +y, 1 - z; [#3] 2 - x, 1 - y, 1 - z.

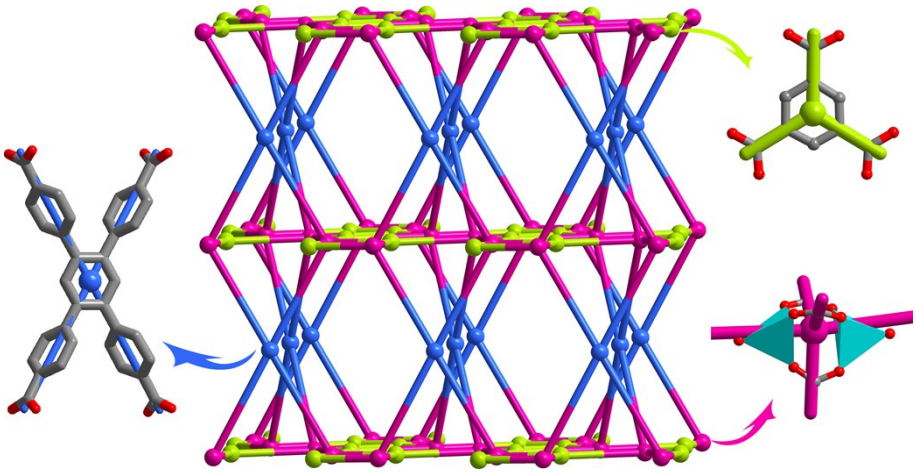

Fig. S2. Topological structure of **JOU-44**.

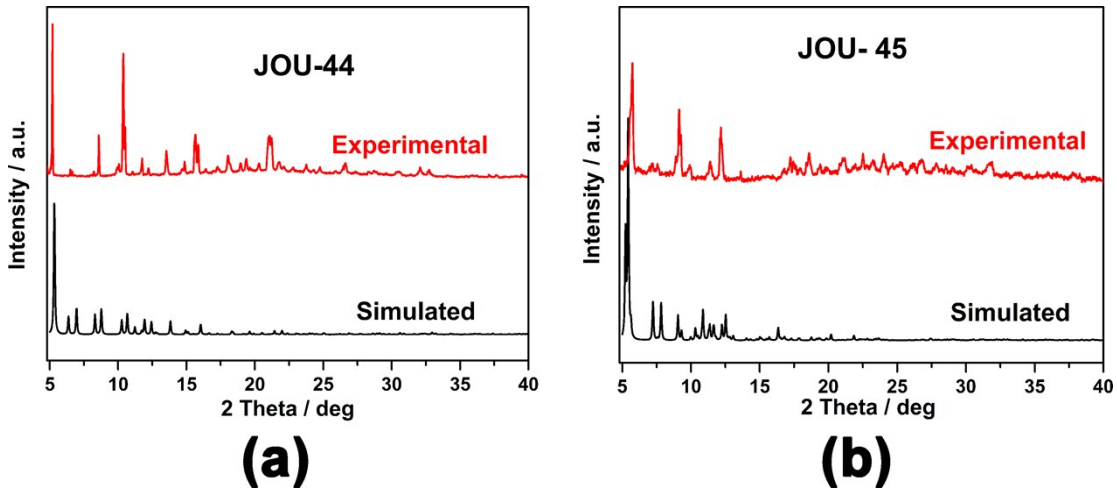

Fig. S3. PXRD patterns of **JOU-44** (a) and **JOU-45** (b).

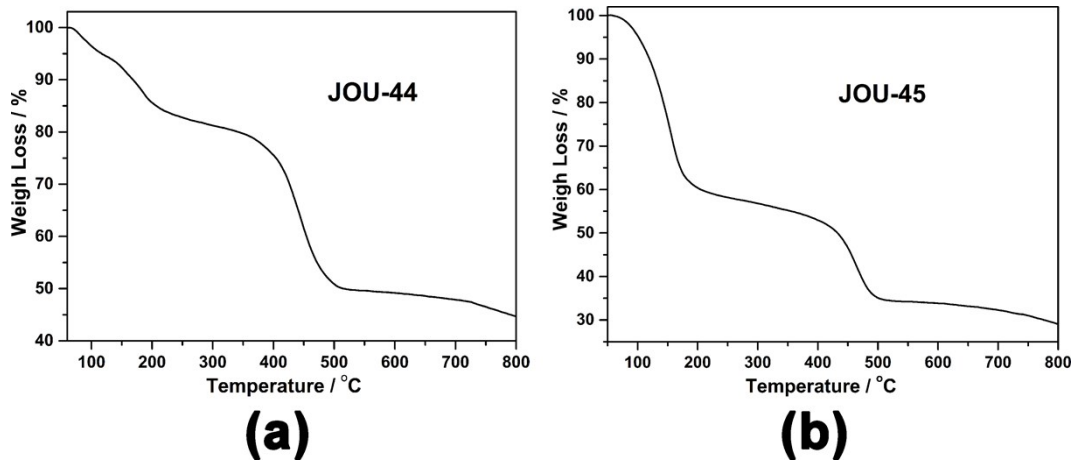

Fig. S4. TG curve of **JOU-44** (a) and **JOU-45** (b).

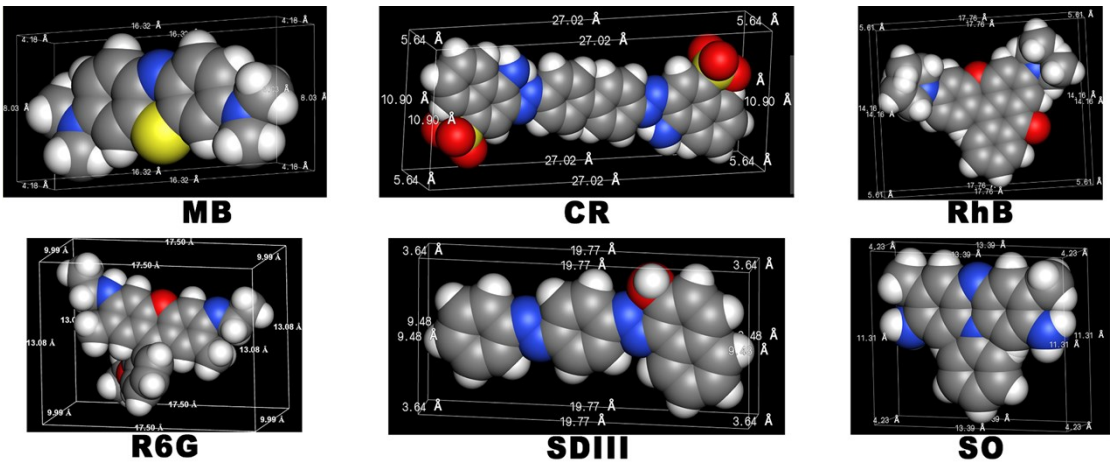

Fig. S5. Representation of the sizes of MB, R6G, RhB, SO, CR and SDIII. The sizes of these dyes are smaller than the channel size of **JOU-44**.

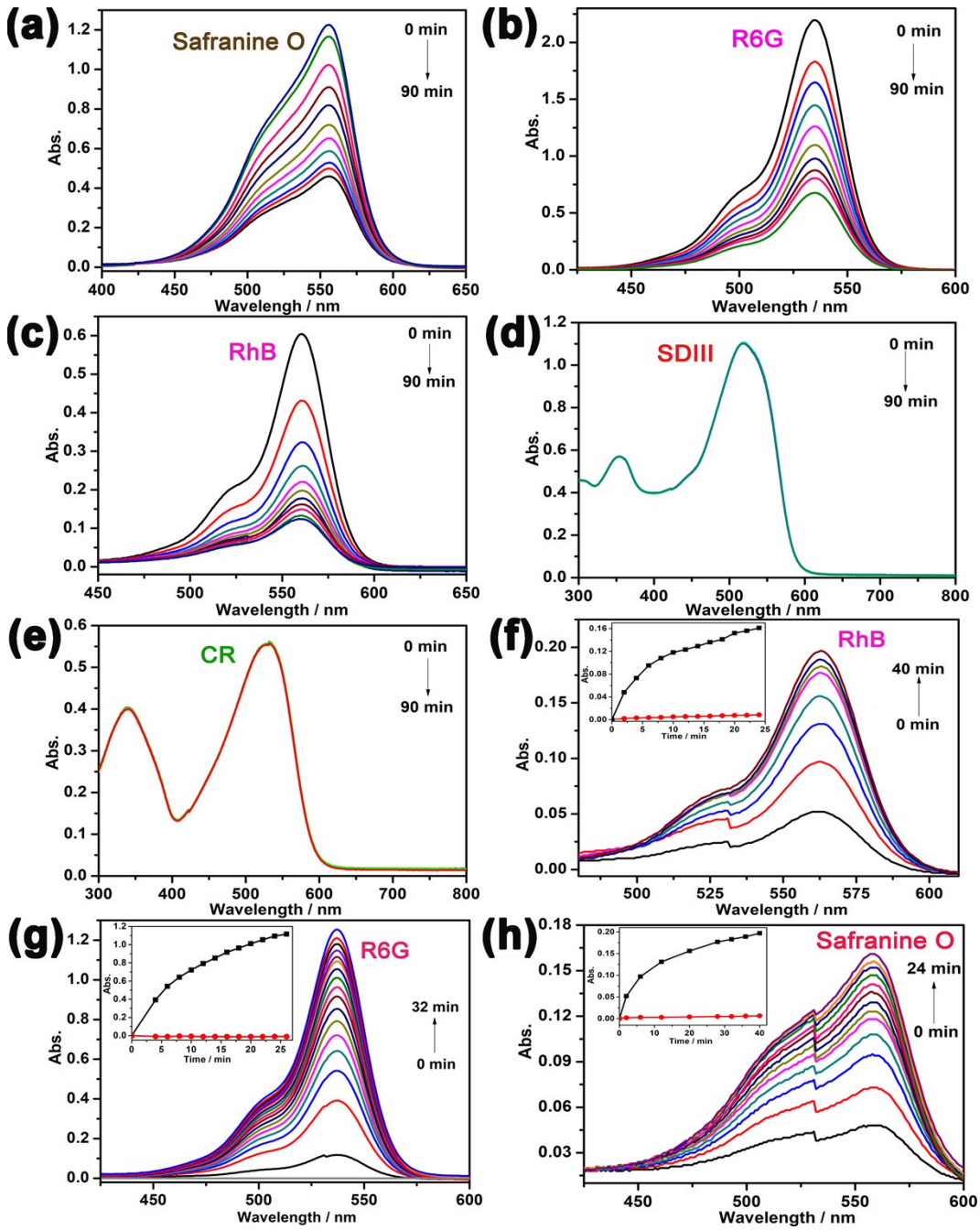

Fig. S6. Adsorption behaviors of **JOU-44** toward SO (a), R6G (b), RhB (c), SDIII (d), and CR (e). Releasing behaviors of dye loaded **JOU-44** toward RhB (f), R6G (g), and SO (h).

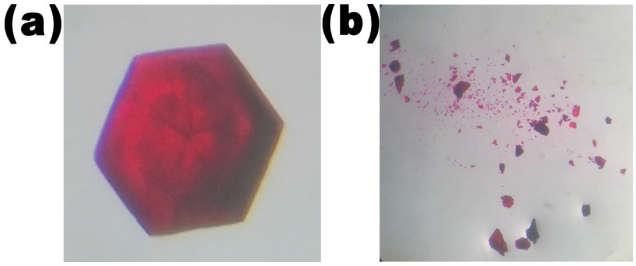

Fig. S7. Photos of R6G@**JOU-44** crystal (a) and crushed R6G@**JOU-44** crystal (b).

Table S4 Comparison of MB adsorption capacity in MOF materials.

Materials	Capacity (mg g^{-1})	Ref.
FJI-C2	1323	5
LIFMWZ-3	983	6
MOP-1	712.2	7
NBC800-3	436	8
Zn-MOF	326	9
JOU-44	208.826	This work
αMOC-1	150	10
Tb-MOF	147	11
Eu-MOF	141	11
CSB	129.44	12
Cu-BTC	42.3	13
NENU-505	33.5	14

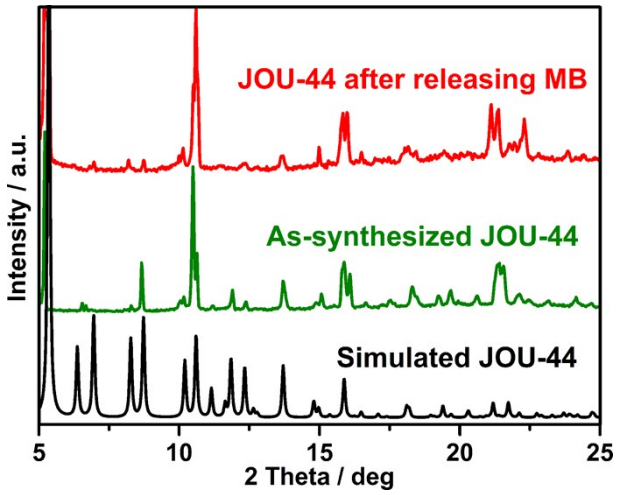

Fig. S8. Stability of **JOU-44** after releasing MB.

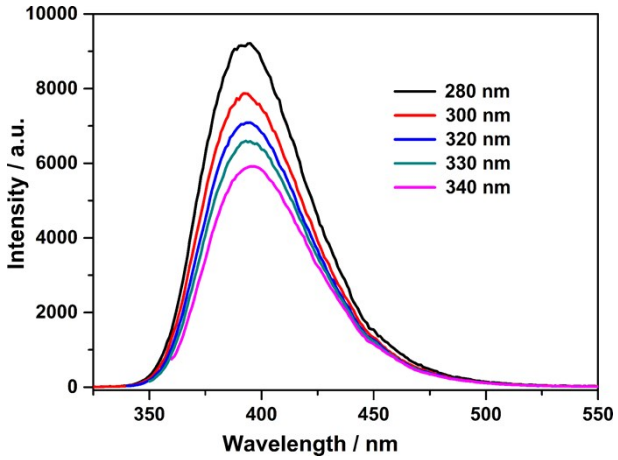

Fig. S9. The emission spectra of **JOU-44** under different excitation wavelengths.

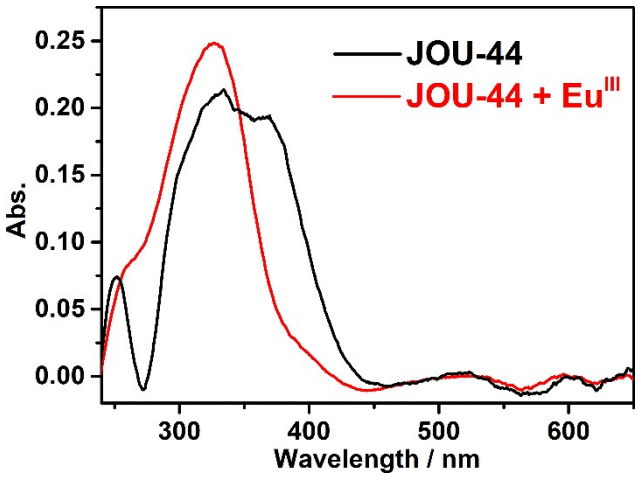

Fig. S10. The solid UV-vis spectra of **JOU-44** and Eu^{III}@**JOU-44**.

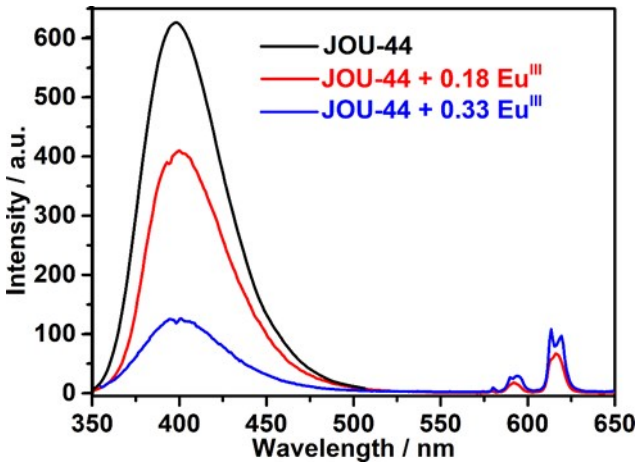

Fig. S11. The emission spectra of **JOU-44** and Eu^{III}@**JOU-44**. As the loading amount of Eu^{III} ions increased, the emission intensity of **JOU-44** gradually decreased while the emission intensity of Eu^{III} ions increased, suggesting the sensitization of Eu^{III} ions.

Reference

1. D. Alezi, A. M. Peedikakkal, L. J. Weselinski, V. Guillerm, Y. Belmabkhout, A. J. Cairns, Z. Chen, L. Wojtas, M. Eddaoudi, Quest for highly connected metal-organic framework platforms: rare-earth polynuclear clusters versatility meets net topology needs, *J. Am. Chem. Soc.*, 2015, **137**, 5421-5430.
2. I. A. Ibarra, P. A. Bayliss, E. Pérez, S. Yang, A. J. Blake, H. Nowell, D. R. Allan, M.Poliakoff, M. Schröder, Near-critical water, a cleaner solvent for the synthesis of a metal-organic framework, *Green Chem.*, 2012, **14**, 117-122.
3. (a) G. M. Sheldrick, *Acta Crystallogr. A*, 2008, **A64**, 112-122; (b) G. M. Sheldrick, *Acta Crystallogr. C*, 2015, **C71**, 3-8.
4. A. L. Spek, *J. Appl. Crystallogr*, 2003, **36**, 7-13.
5. X. S. Wang, J. Liang, L. Li, Z. J. Lin, P. P. Bag, S. Y. Gao, Y. B. Huang, R. Cao, An Anion Metal-Organic Framework with Lewis Basic Sites-Rich toward Charge-Exclusive Cationic Dyes Separation and Size-Selective Catalytic Reaction, *Inorg. Chem.*, 2016, **55**, 2641-2649.
6. Z. Wang, J. H. Zhang, J. J. Jiang, H.-P. Wang, Z. W. Wei, X. Zhu, M. Pan, C. Y. Su, A stable metal cluster-metalloporphyrin MOF with high capacity for cationic dye removal. *J. Mater. Chem. A*, 2018, **6**,17698-17705.
7. B. Wang, Q. Zhang, G. Xiong, F. Ding, Y. He, B. Ren, L. You, X. Fan, C. Hardacre, Y. Sun, Bakelite-type anionic microporous organic polymers with high capacity for selective adsorption of cationic dyes from water, *Chem. Eng. J.*, 2019, **366**, 404-414.
8. F. Lian, G. Cui, Z. Liu, L. Duo, G. Zhang, B. Xing, One-step synthesis of a novel N-doped microporous biochar derived from crop straws with high dye adsorption capacity, *J Environ. Manage.*, 2016, **176**, 61-68.
9. J. Zhang, F. Li, Q. Sun, Rapid and selective adsorption of cationic dyes by a unique metal-organic framework with decorated pore surface, *Appl. Surf. Sci.*, 2018, **440**, 1219-1226.
10. Y. Gao, S. Q. Deng, X. Jin, S. L. Cai, S. R. Zheng, W. G. Zhang, The construction of amorphous metal-organic cage-based solid for rapid dye adsorption and time-dependent dye separation from water, *Chem. Eng. J.*, 2019, **357**, 129-139.
11. Z. Cui, X. Zhang, S. Liu, L. Zhou, W. Li, J. Zhang, Anionic Lanthanide Metal-Organic Frameworks: Selective Separation of Cationic Dyes, Solvatochromic Behavior, and Luminescent Sensing of Co(II) Ion, *Inorg. Chem.*, 2018, **57**, 11463-11473.
12. S. Chatterjee, T. Chatterjee, S. R. Lim, S. H. Woo, Adsorption of a cationic dye, methylene blue, on to chitosan hydrogel beads generated by anionic surfactant gelation, *Environ. Technol.*, 2011, **32**, 1503-1514.
13. R. Kaur, A. Kaur, A. Umar, W. A. Anderson, S. K. Kansal, Metal organic framework (MOF) porous octahedral nanocrystals of Cu-BTC: Synthesis, properties and enhanced adsorption properties, *Mater. Res. Bull.*, 2019, **109**, 124-133.
14. S. R. Zhang, J. Li, D. Y. Du, J. S. Qin, S. L. Li, W. W. He, Z. M. Su, Y. Q. Lan, A multifunctional microporous anionic metal-organic framework for column-chromatographic dye separation and selective detection and adsorption of Cr^{3+}, *J. Mater. Chem. A*, 2015, **3**, 23426-23434.